Making Sense of a Missense Mutation: Characterization of MutT2, a Nudix Hydrolase from *Mycobacterium tuberculosis*, and the G58R Mutant Encoded in W-Beijing Strains of *M. tuberculosis*[†]

Nicole J. Moreland,*[,‡] Caroline Charlier,[⊥,‡] Andrew J. Dingley,[‡,§] Edward N. Baker,[‡] and J. Shaun Lott*[,‡,||]

Maurice Wilkins Centre for Molecular Biodiscovery and Laboratory of Structural Biology, School of Biological Sciences, University of Auckland, New Zealand, Department of Chemistry, University of Auckland, New Zealand, and AgResearch Structural Biology Laboratory, School of Biological Sciences, University of Auckland, New Zealand

Received May 21, 2008; Revised Manuscript Received October 9, 2008

ABSTRACT: Recent polymorphism analyses of *Mycobacterium tuberculosis* strains have identified missense mutations unique to the W-Beijing lineage in genes belonging to the Nudix hydrolase superfamily. This study investigates the structure and function of one of these Nudix hydrolases, MutT2, and examines the effect that the W-Beijing mutation (G58R) has on enzyme characteristics. MutT2 has a preference for cytidine triphosphates, and although the G58R mutation does not alter nucleotide specificity, it reduces the protein's affinity for divalent cations. The K_D of free Mg^{2+} is 79-fold higher for the G58R mutant (3.30 ± 0.19 mM) compared with that for the wild-type (41.7 ± 1.4 μM). Circular dichroism and nuclear magnetic resonance spectroscopy measurements show that while the mutation does not perturb the overall structure of the protein, protein stability is significantly compromised by the presence of the arginine with ΔG (H_2O), the free-energy of unfolding, being reduced by 2.48 kcal mol^{-1} in the G58R mutant. Homology modeling of MutT2 shows that Gly-58 is in close proximity (10.8 Å) to the Mg^{2+} binding site formed by the highly conserved Nudix box residues and hydrogen bonds with Ala-54 in the preceding α-helix. This may explain the increased divalent cation requirement and decreased stability observed when an arginine is substituted for glycine at this position. A role for MutT2 in the regulation of cytidine-triphosphates available for nucleotide-dependent reactions is postulated, and the impact that the G58R mutation may have on these reactions is discussed.

Tuberculosis (TB[1]), an infectious disease responsible for the deaths of 1.6 million people each year, is caused by different strains of *Mycobacterium tuberculosis* with varying degrees of virulence. Of these, the W-Beijing family of strains is particularly successful and has been associated with many major TB outbreaks in recent years. The W-Beijing strains are thought to have originated in China, but are now disseminating throughout the world, having been implicated in epidemics in the USA, South Africa, Russia, and Spain (*1, 2*). They exhibit strong pathological features such as multidrug resistance, high virulence, and exogenous reinfection, and display altered expression of antigens, virulence factors, and glycolipids, which may be important factors in determining their success (*1*).

Two recent studies have investigated the variation in putative DNA repair genes from the *mutT* family in clinical isolates of W-Beijing *M. tuberculosis* (*3, 4*). Resistance to antimycobaterial drugs occurs, almost exclusively, as a result of genomic mutations in specific genes (*5, 6*). In other bacteria, mutated phenotypes commonly result from defects in DNA repair and it has been hypothesized that W-Beijing strains may have defective DNA repair systems, allowing an increased mutation rate that, in turn, would lead to a selective advantage during drug exposure and niche adaptation (*4*). A polymorphism analysis of 139 *M. tuberculosis* strains (including 55 with a W-Beijing genotype) found alterations in two putative *mutT* genes (Rv1160 (*mutT2*) and Rv3908, designated by the authors to be *mutT4*) that were characteristic and unique to the W-Beijing lineage (*4*). Each of the mutations would result in a nonconservative amino acid change in the encoded protein, G58R in *mutT2* and R48G in *mutT4*. A second, smaller analysis of 30 W-Beijing strains confirmed the presence of these specific missense mutations in the Beijing lineage but did not find a significant association between the presence of the mutations and whether the strains displayed drug resistance (*3*). The authors suggest that this does not discount the possibility that the

[†] This work was supported by the New Economy Research Fund of New Zealand and Centers of Research Excellence funding to the Maurice Wilkins Centre of Molecular Biodiscovery. C.C. is the recipient of a Postdoctoral Fellowship from the Belgian Fund for Scientific Research (FRS-FNRS).

* To whom correspondence should be addressed. Phone: +64-9-373-7599. Fax: +64-9-373-7619. E-mail: n.moreland@mac.com (N.J.M.); s.lott@auckland.ac.nz. (J.S.L.).

[‡] Maurice Wilkins Centre for Molecular Biodiscovery and Laboratory of Structural Biology.

[§] Department of Chemistry.

[||] AgResearch Structural Biology Laboratory.

[⊥] Present address: CBS Laboratory, University of Namur, Namur, Belgium.

[1] Abbreviations: TB, tuberculosis; *Ec*MutT, *E. coli* MutT; *Mt*MutT2, *M. tuberculosis* MutT2; IMAC, immobilized metal ion affinity chromatography; SEC, size exclusion chromatography; rTEV, recombinant tobacco etch virus, PPi, pyrophosphate; 3D, three-dimensional; NTP nucleotide-triphosphate.

10.1021/bi8009554 CCC: $40.75
Published on Web 12/30/2008

mutations contribute to a mutator phenotype but that the phenotype might only appear when strains are subject to the selective pressure of antimycobacterial therapy. However, there is an alternative explanation for the lack of mutator phenotype observed, that the proteins encoded by the putative *mutT* genes do not function as part of a DNA repair pathway.

The *mutT* genes in *M. tuberculosis* have been annotated as such because they encode a highly conserved amino acid motif called a Nudix box that is present in *E. coli* MutT (*Ec*MutT) and in all other proteins in the large and diverse Nudix superfamily (*4, 7, 8*). The preferred substrate of *Ec*MutT, the prototypical member of the Nudix family, is the oxidatively damaged nucleotide 8-oxo-dGTP. Incorporation of this nucleotide into DNA can cause mispairing leading to transitions and transversions, and *Ec*MutT prevents DNA damage by hydrolyzing the damaged nucleotide (*9*). However, other Nudix enzymes have been shown to hydrolyze a wide range of organic pyrophosphates including nucleoside di- and triphosphates, nucleotide sugars and alcohols, dinucleoside polyphosphates, dinucleotide coenzymes, and capped RNA, many of which are in no way involved in, or result in, DNA damage. Commonality in function across the diverse superfamily is limited to the broad observation that the enzymes act on nucleoside diphosphates linked to another moiety, X. The residues that form the Nudix box, $Gx_5Ex_5UxREUxEExGU$ (where U is a hydrophobic amino acid, and x stands for any residue), do not participate in the binding of substrate but coordinate catalytically essential Mg^{2+} ions (reviewed in *10*−*12*).

In the present study, we have investigated the structure and function of *M. tuberculosis* MutT2 (*Mt*MutT2) and the G58R mutant protein observed in W-Beijing strains. On the basis of sequence similarity with *Ec*MutT, *Mt*MutT2 has been annotated as a probable mutator protein and an 8-oxo-dGTPase (http://genolist.pasteur.fr/TubercuList/). However, we show that it has a preference for cytidine triphosphates, rather than guanosine triphosphates. The W-Beijing mutation (G58R) maps to the last glycine in the conserved Nudix box ($Gx_5Ex_5UxREUxEEx\mathbf{G}U$), and we have explored the effect this mutation has on nucleotide hydrolysis, Mg^{2+} dependence, and protein stability. The results reveal that significant differences in these properties are caused by the single amino acid substitution. With the aid of a homology model of *Mt*MutT2, we have examined the effects the G58R mutation may have on molecular structure and discuss the potential impact of the mutation on the bacterium *in vivo*.

EXPERIMENTAL PROCEDURES

Cloning and Mutagenesis of MtMutT2. The ORF encoding *Mt*MutT2 (Rv1160) was amplified by nested PCR from *M. tuberculosis* H37Rv genomic DNA and cloned using Gateway cloning methods as published previously (*13*). Briefly, first round PCR was performed with primers containing 15−18 base pairs of gene specific sequence and 12 base pairs that overlap with the second round generic primers. The generic primers contain *attB* sequences necessary for subsequent Gateway cloning. First round PCR primer sequences were forward, 5′-GGCAGCGGCGCGATGCTGAATCAGATC-3′; reverse, 5′-GAAAGCTGGGTG;CTAACAGCGACGGTGGAC-3′. The gene specific sequence is underlined. Following second round PCR with generic primers, the amplified product was purified using a spin column (Qiagen). A BP reaction[2] was performed with the *att*B-flanked PCR product and pDONR221 (Invitrogen) to generate an entry clone. The entry clone was, in turn, subcloned via an LR reaction[2] into pDEST17, an N-terminal His-tag expression vector (Invitrogen).

Site-directed mutagenesis of residues G58R and D119N was carried out using the QuickChange Kit (Stratagene) and pDEST17-Rv1160 as a template. Primer pairs for G58R were forward, 5′-CTCGCCGAAGAACTGCGACTCGAGGTCGCCGAC-3′; reverse, 5′-GTCGGCGACCTCGAGTCGCAGTTCTTCGGCGAG-3′. Primer pairs for D119N were forward, 5′-CTGGGTACCAGCCAACCGCGGCTGGATTG-3′; reverse, 5′-CAATCCAGCCGCGGTTGGCTGGTACCCAG-3′. The nucleotides changed to allow specific amino acid replacement are underlined. Mutations were verified by DNA sequencing.

Expression and Purification of Recombinant Proteins. The expression constructs were transformed into *Escherichia coli* BL21 (DE3) cells and plated on Luria−Bertani agar medium containing 100 μg/mL ampicillin. All *Mt*MutT2 expression was performed in autoinduction media (*14*) supplemented with ampicillin. For the expression of native protein, a single colony was used to inoculate a seeder culture, grown overnight at 37 °C in MDG[3] noninducing medium. The MDG culture was used at a dilution of 1:1000 to seed the autoinduction medium ZYM-5052[3] for expression. For expression of ^{15}N-enriched protein, a single colony was used to inoculate a seeder culture of LSG[3] noninducing medium. Following an overnight incubation at 37 °C, the LSG culture was used at a dilution of 1:40 to seed the ^{15}N-supplemented minimal medium LS-5052[3]. Both ZYM-5052 and LS-5052 expression cultures were routinely grown at 37 °C for 4 h followed by 20 h at 18 °C.

Native and ^{15}N-enriched proteins were purified using immobilized metal ion affinity chromatography (IMAC) followed by size exclusion chromatography (SEC). Cells from *Escherichia coli* BL21 (DE3) expression cultures were harvested by centrifugation (3,500*g*, 15 min, 4 °C). Cell pellets were resuspended in lysis buffer (20 mM Hepes at pH 7.2, 150 mM NaCl, 2 mM β-mercaptoethanol, and 10 mM imidazole) supplemented with two, EDTA-free, protease inhibitor tablets (Roche Applied Science). Resuspended cells were passed through a cell disrupter (Constant Systems Ltd.) set at 18 kpsi and centrifuged at 16,000*g* for 45 min (4 °C). The soluble fraction containing His-tagged *Mt*MutT2 was

[2] BP reaction is a Gateway cloning reaction in which an *attB*-flanked PCR product is recombined with an *attP* substrate (pDONR221; Invitrogen) using BP Clonase (Invitrogen) to generate an entry clone. LR reaction is a Gateway cloning reaction in which an entry clone containing *attL* sequences is recombined with an *attR* destination vector using LR Clonase (Invitrogen).

[3] MDG, noninducing medium comprising 25 mM Na_2HPO_4, 25 mM KH_2PO_4, 50 mM NH_4Cl, 5 mM Na_2SO_4, 2 mM $MgSO_4$, 0.2× trace metals, 0.5% glucose, and 0.25% aspartate; ZYM-5052, autoinduction medium comprising 1% N-Z-amine AS, 0.5% yeast extract, 25 mM Na_2HPO_4, 25 mM KH_2PO_4, 50 mM NH_4Cl, 5 mM Na_2SO_4, 2 mM $MgSO_4$, 1× trace metals, 0.5% glycerol, 0.05% glucose, and 0.2% α-lactose; LSG, noninducing medium comprising 12.5 mM Na_2HPO_4, 12.5 mM KH_2PO_4, 50 mM NH_4Cl, 5 mM Na_2SO_4, 2 mM $MgSO_4$, 0.2× trace metals, 0.5% glucose, and 20 mM succinate; LS-5052, ^{15}N-supplemented minimal media comprising 12.5 mM Na_2HPO_4, 12.5 mM KH_2PO_4, 50 mM $^{15}NH_4Cl$, 5 mM Na_2SO_4, 2 mM $MgSO_4$, 1× trace metals, 0.5% glycerol, 0.05% glucose, 0.2% α-lactose, and 20 mM succinate.

loaded onto a Ni-NTA column (Amersham Biosciences) pre-equilibrated with lysis buffer. Captured *Mt*MutT2 was eluted with an imidazole gradient of 10−700 mM. Fractions containing *Mt*MutT2 were incubated overnight at 4 °C with 1 mg of recombinant tobacco etch virus (rTEV) protease to remove the His-tag prior to further purification by SEC using a Superdex75 10/300 column. The standard SEC buffer was 20 mM Hepes at pH 7.2, 150 mM NaCl, and 2 mM β-mercaptoethanol, but this was varied depending on the down-stream application of the protein as detailed below. Fractions from Superdex75 containing *Mt*MutT2 were concentrated as required using a centrifugal concentrator (Vivaspin 5,000 MWCO).

Circular Dichroism. Circular dichroism (CD) spectra in the far-UV region (200 to 260 nm) were obtained at 24 °C with a PiStar spectrometer (Applied PhotoPhysics) in a 0.1 cm quartz cell. All protein samples were purified by SEC in 10 mM sodium phosphate at pH 7.2 and concentrated to 10 μM. Measured circular dichroism ellipticity values were converted to mean residue ellipticity [θ] in deg cm^2 decimol^{-1} using the equation $[\theta] = 100\Delta\theta/Cnl$ where $\Delta\theta$ is the difference in millidegrees between the protein sample and buffer alone, C is the protein concentration (mM), n is the number of residues in the protein, and l is the path length of the cuvette (cm).

The stabilities of wild-type *Mt*MutT2 and the G58R mutant were determined from urea denaturation curves produced from circular dichroism measurements at 218 nm. The urea used was Sequenal grade (Pierce), and each sample was incubated for at least 2 h before measurements were made to ensure the folding reaction had reached equilibrium. Analysis of the denaturation curves was performed using the two-state folding model and the linear extrapolation method (*15*), where the fraction of unfolded protein (f_U) at a given urea concentration is calculated as $f_U = (y_F - y)/(y_F - y_U)$, where y is the measured value (θ), and y_F and y_U are values of y in the folded and unfolded states, respectively. Experimental curves were fitted to this equation using SigmaPlot data analysis software v10 (Systat Software Inc.). Denaturation curves were performed at least three times for both the wild-type and mutant proteins. Using the fitted data, the equilibrium constant, K, between the folded and unfolded forms of the protein and the corresponding free energy change, ΔG, were calculated using $K = f_U/(1 - f_U)$ and $\Delta G = -RT \ln K$, where R is the gas constant, and T is the absolute temperature. Plots of ΔG versus the urea concentration were fitted by linear regression according to the two-state model in which $\Delta G = \Delta G\ (H_2O) - m[\text{urea}]$, where $\Delta G\ (H_2O)$ is the free-energy of unfolding in the absence of urea, and m is the measure of ΔG dependence on urea. The midpoint of denaturation, C_m, corresponds to the urea concentration where $\Delta G = 0$.

Nuclear Magnetic Resonance Spectroscopy. All protein samples intended for NMR analysis were purified by SEC in 10 mM Hepes at pH 7.2, 50 mM NaCl, 2 mM Tris (2-carboxyethyl) phosphine hydrochloride (TCEP), and concentrated to 70 μM. Following the addition of D_2O to 7% (v/v), $^1H-^{15}N$ HSQC spectra were recorded at 25 °C on a Bruker AV600 NMR spectrometer equipped with a z-axis pulsed-field gradient $^1H/^{15}N/^{13}C$ cryoprobe optimized for ^1H detection. Data matrices consisted of 128* × 1024* data points (were n* refers to complex points) with acquisition times of 62 (t_N) and 136 ms (t_{HN}). A total of 128 scans per complex t_N increment were collected, and the total measuring time for each experiment was 5.5 h. Data sets were processed using NMRPipe (*16*) and spectra visualized using CcpNmr Analysis (*17*).

Enzyme Assays. Hydrolysis of the substrates and release of pyrophosphate (PPi) was measured using a colorimetric method adapted from Ames and Dubin (*18*). This method is routinely used to detect Pi, but we and others have found that by extending the incubation time in the colorimetric step it can also be used to reliably measure PPi (*19, 20*). All protein samples were purified in the standard SEC buffer and concentrated to 180 μM. Standard reactions contained 50 mM Tris-HCl at pH 8.0, 15 mM $MgCl_2$, 25 mM NaCl, 2.5 mM substrate, and 5 μM of enzyme in a final volume of 30 μL. Reactions were incubated at 37 °C for 25 min and stopped by the addition of 100 mM EDTA. The reaction mixture (25 μL) was transferred into 125 μL of reagent A (four parts 10% w/v ascorbate and one part ammonium molybdate in 15 mM zinc acetate at pH 5.0) and incubated at 45 °C for 45 min. A_{710} was determined using a SpectraMAX microplate reader (Molecular devices), and all absorbance readings were corrected for enzyme-unrelated absorbance change. The amount of PPi released was determined with a standard curve, and all assays were carried out in triplicate.

The colorimetric assay was used to determine kinetic parameters (V_{max} and K_m) toward dCTP and the affinity constant (K_D) toward Mg^{2+} for wild-type and G58R *Mt*MutT2. To ensure that K_D represents affinity for enzyme-bound metal, Mg^{2+} concentration was corrected for nucleotide bound metal using a K_D of 10 μM for Mg^{2+}-dCTP (*21*). The data were fitted to the Michaelis−Menten equation, and kinetic constants were calculated using SigmaPlot v10 (Systat Software Inc.).

Anion-exchange HPLC was used to quantify the ratio of substrate to product formed in the enzyme reactions as previously described (*22*). Following the incubation of a 30 μL reaction at 37 °C and the addition of 100 mM EDTA to stop the reaction as above, aliquots were loaded onto a MonoQ column (GE Healthcare) pre-equilibrated with 2 mM NaOH. Elution of the products (and remaining substrate) was achieved with a gradient of 0−100% of buffer comprising 2 mM NaOH and 1 M sodium acetate. Detection was performed with UV absorbance at 260 nm.

Homology Model of MtMutT2. A three-dimensional (3D) homology model of *Mt*MutT2 was built on the basis of the NMR structure of *Ec*MutT bound to Mg^{2+} and 8-oxo-dGMP (PDB accession code 1PUQ (*23*)) using ESyPred3D (*24*). This program derives a consensus alignment between the target and template sequences, on the basis of the results of several alignment algorithms, and uses the modeling package MODELER (*25*) to build the final 3D structure. The metal binding site was located using GRID (*26*) and an Mg^{2+} probe. Figures were created with Pymol (www.pymol.org).

RESULTS AND DISCUSSION

MtMutT2 and Related Nudix Hydrolases. A BLAST search of the *M. tuberculosis* genome using *Ec*MutT as the amino acid query sequence returned nine related sequences. All contained the highly conserved Nudix box amino acids, but

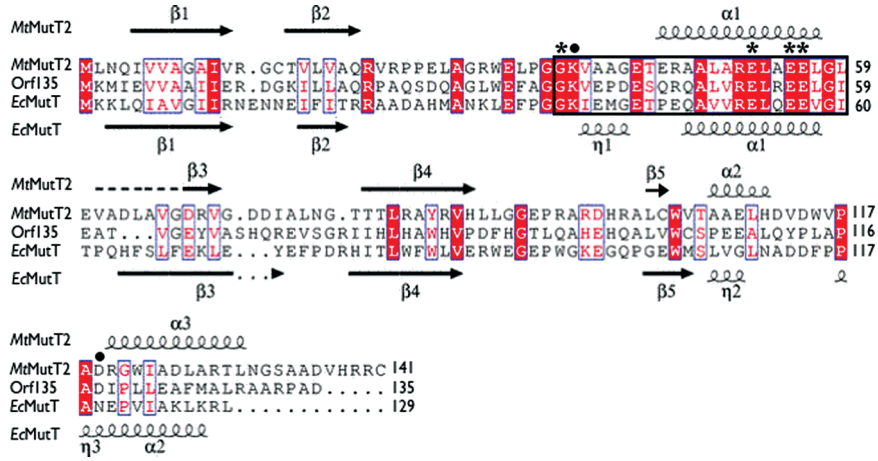

FIGURE 1: Alignment of *Mt*MutT2 and the related *E. coli* Nudix hydrolases *Ec*MutT and Orf135. Alignments were prepared with ClustalW (*49*). The secondary structure prediction for *Mt*MutT2 was generated using PSIPRED (*50*) and is shown above. Secondary structure elements from the *Ec*MutT NMR structure (PDB accession code 1PUQ) are shown below. Conserved Nudix box is outlined in black, and divalent metal binding residues (*) and active site residues (●) are as indicated.

outside this short stretch of conservation, the sequences were extremely variable and differed in length by over 200 amino acids. Only *Mt*MutT2 showed significant sequence conservation with *Ec*MutT over the entire sequence length (Figure 1), and being the closest match, with an overall sequence identity of 27% (*E*-value = 2.7×10^{-10}), it appears reasonable that *Mt*MutT2 has been annotated as a probable mutator protein and an 8-oxo-dGTPase (http://genolist.pasteur.fr/TubercuList/). However, when *Mt*MutT2 was used as the query sequence in a BLAST search of the *E. coli* genome, a protein named Orf135 was identified as the closest match with an overall sequence identity of 39% (*E*-value = 2.0×10^{-10}). *Ec*MutT was the second closest match (*E*-value = 8.0×10^{-08}). Furthermore, a reciprocal BLAST search of the *M. tuberculosis* genome using Orf135 as the query sequence identified *Mt*MutT2 as the closest match (*E*-value = 7.0×10^{-12}). Like *Ec*MutT, Orf135 contains the highly conserved Nudix box residues, but it has been shown to have specificity for cytidine triphosphates, rather than guanosine triphosphates (*27*). An alignment of *Mt*MutT2 with *Ec*MutT and Orf135 illustrates the higher level of conservation between *Mt*MutT2 and Orf135 (Figure 1). Therefore, although *Mt*MutT2 is designated an 8-oxo-dGTPase, sequence analysis suggests that it may be more like the *E. coli* Nudix hydrolase Orf135. To test this, we investigated the substrate specificity and kinetic properties of *Mt*MutT2.

The specific missense mutation (G58R) found in *Mt*MutT2 in the highly virulent W-Beijing strains maps to the last glycine of the conserved Nudix box (Figure 1). The residues of the Nudix box form part of a conserved loop−helix−loop structural motif seen in all members of the Nudix superfamily for which structural information is available (*10, 11, 28*). To examine the likely structural effects of the G58R mutation, we have generated a homology model of *Mt*MutT2 using MODELER (*25*) with the most recent NMR structure of *Ec*MutT as a template (PDB accession code 1PUQ (*23*)). Although the sequence identity between the two proteins is only 27% overall, the 23 residue Nudix box region is highly conserved with a sequence identity of 52% (Figure 1), giving confidence that it can be modeled accurately. *Mt*MutT2 is predicted to form an α/β/α sandwich like *Ec*MutT, with the Nudix box mapping to the helix within the conserved loop−helix−loop structural motif shown in Figure 2A. The Nudix box residues do not participate in binding of the substrate but have been shown to coordinate a catalytically essential Mg^{2+} ion (*10, 11*). In *Ec*MutT (Figure 2A), Gly-38 and Glu-53, Glu-56, and Glu-57 within the Nudix box (together with two water molecules) coordinate the divalent cation (*23, 28*), and mutations of the corresponding residues to alanine in Orf135 markedly reduced activity (*29*). An independent prediction of the metal binding site in *Mt*MutT2, using GRID (*26*) and an Mg^{2+} probe, pointed to the same residues (Gly-37 and Glu-52, Glu-55 and Glu-56) providing validation of the accuracy of this region of the homology model (Figure 2B).

Gly-58, the residue mutated to arginine in the W-Beijing strains, forms part of a tight turn following the conserved helix in our model (Figure 2B), as does the corresponding residue in *Ec*MutT (Gly-59; Figure 2A) (*23*). The residues have (φ, Ψ) values that place them in a region of the Ramachandran plot that is disallowed for nonglycine residues; ($\varphi = 61$ °, $\Psi = -55$ °) for *Mt*MutT2 Gly-58 and ($\varphi = 67$ °, $\Psi = -33$ °) for *Ec*MutT Gly-59. Substitution of glycine by the more bulky arginine residue at this position would introduce steric constraints on the backbone of the turn that may disturb the end of the conserved helix and consequently the coordination of Mg^{2+}. We set out to experimentally investigate this predicted structural disturbance and establish its consequences on protein stability and substrate specificity.

Biophysical Properties of WT and G58R Mutant MtMutT2. MtMutT2 and the G58R mutant protein were purified by IMAC using the poly histidine tag attached to the N-terminus of the fusion proteins. The His-tags were subsequently removed with rTEV protease before further purification using SEC. Following SEC, both proteins were >95% pure as judged by SDS−PAGE analysis with no evidence of proteolysis. Both the wild-type and the G58R mutant protein eluted as a single peak that corresponds to the predicted molecular weight for an *Mt*MutT2 monomer (15 kDa, data not shown). *Ec*MutT and Orf135 have also been shown to be monomeric in solution (*27, 30*).

We examined the spectroscopic properties of the wild-type and G58R mutant proteins using far-UV CD and NMR ($^1H-^{15}N$ HSQC spectra) to assess the effects the W-Beijing

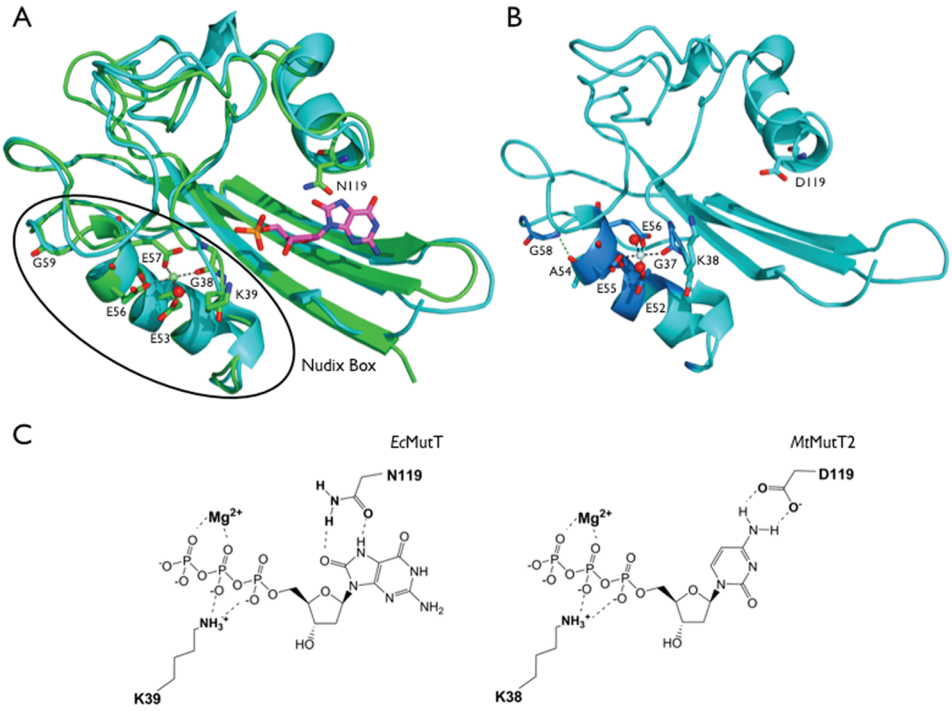

FIGURE 2: (A) Superposition of *Ec*MutT (green; PDB 1PUQ) onto the homology model of *Mt*MutT2 (cyan). 8-oxo-GMP from the *Ec*MutT NMR structure is shown in pink. (B) Homology model of *Mt*MutT2. Conserved Nudix box residues are highlighted in dark blue. (C) Chemical structures of the preferred substrates and nucleotide binding residues for *Ec*MutT (8-oxo-dGTP) and *Mt*MutT2 (dCTP).

mutation has on secondary structure. The far-UV CD spectrum of *Mt*MutT2 (Figure 3A) shows minima of negative ellipticity at 208 and 218 nm, typical of a protein with considerable content of both α-helix and *β*-sheet (*31*). The CD spectrum for the mutant protein is essentially superimposable on that of the wild-type, and an estimation of the proportion of secondary structure elements using CDNN (*32*) showed no significant differences between wild-type and G58R (27% α-helices, 40% *β*-sheet and turns, and 33% random coil).

To provide additional information about specific residues in *Mt*MutT2, two-dimensional $^{1}H-^{15}N$ HSQC spectra were collected from ^{15}N-enriched samples. The spectra for both wild-type and G58R show good dispersion of peaks indicative of a well structured protein (Figure 3B) (*33, 34*). The resonance for Gly-58 has been assigned in the wildtype spectrum on the basis that it is absent in the G58R spectrum and is observed in the chemical shift range typically occupied by glycine residues. While the majority of resonances in the two spectra overlay, there are several distinct differences in G58R compared with the wild-type. Taken together with the CD spectra, this suggests that although the overall fold of the protein is unchanged, the local environment of some residues has been altered by the introduction of the mutation. It seems likely that these residues would be located at the end of the conserved helix and in the following loop in *Mt*MutT2 (Figure 2B), but without complete assignment information, we are unable to show this definitively.

MtMutT2 Has Specifity for Cytidine-Triphosphates. The substrate specificity of wild-type and G58R *Mt*MutT2 were determined using modifications of a previously described colorimetric end point assay (*18*). Both wild-type and the G58R mutant show an identical activity profile against a range of nucleotides (Figure 4A). Like *Ec*MutT, *Mt*MutT2

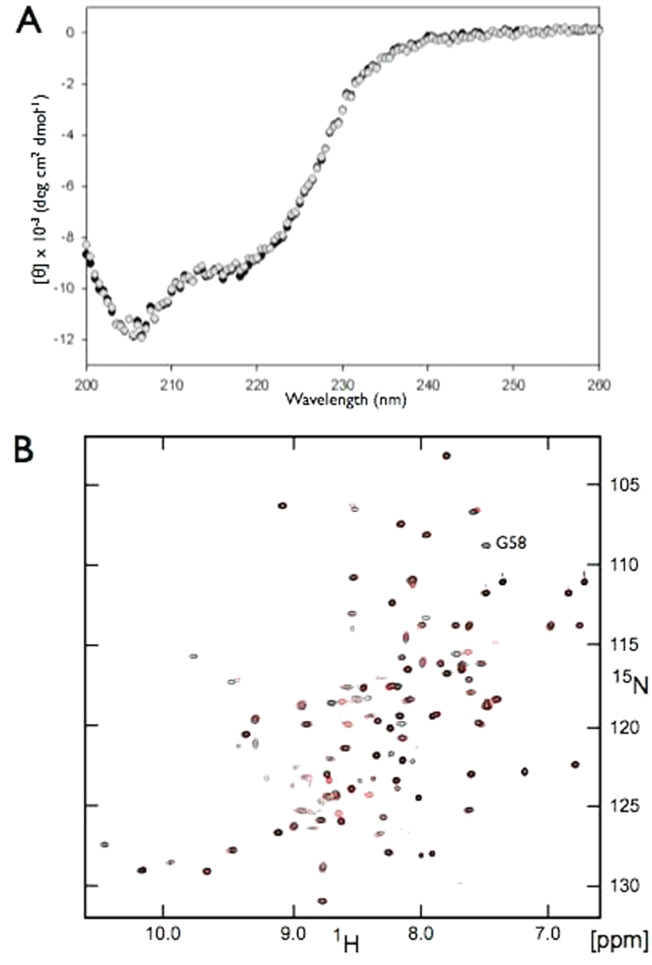

FIGURE 3: (A) Far-UV CD spectra of wild-type (●) and G58R (○) *Mt*MutT2. (B) $^{1}H-^{15}N$ HSQC spectra of wild-type (black) and G58R (red) *Mt*MutT2.

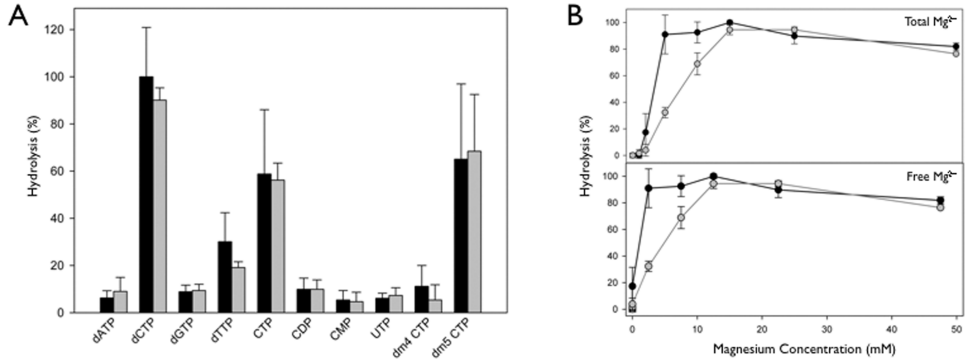

FIGURE 4: (A) Substrate specificity of wild-type (black) and G58R (gray) *Mt*MutT2. All substrates were present at a concentration of 2.5 mM, and the concentration of $MgCl_2$ was saturating at 15 mM. There is no significant difference between wild-type and G58R hydrolysis for all nucleotides ($p > 0.05$ in each *t*-test). (B) Magnesium dependence of wild-type (black) and G58R (gray) *Mt*MutT2. The concentration of substrate (dCTP) was constant at 2.5 mM. The lower curve has been corrected for nucleotide-bound Mg^{2+} and shows magnesium dependence as a function of the free Mg^{2+} concentration.

is capable of hydrolyzing (deoxy)ribonucleoside triphosphates but with markedly different substrate specificity. Whereas *Ec*MutT has a preference for guanosine triphosphates (8-oxo-dGTP, dGTP, and GTP) (*9, 35*), *Mt*MutT2 has a preference for cytidine triphosphates (CTP, dCTP, and 5-methyl-dCTP) (Figure 4A). The specificity for cytidine triphosphates is the same as that observed for Orf135 (*27*) and is confirmation of the bioinformatic prediction that *Mt*MutT2 is not an 8-oxo-dGTPase, but rather a cytidine triphosphatase. As with Orf135, the presence of a hydroxyl group at the C2′ position on the ribose does not have a large effect on activity since marked hydrolysis of both CTP and dCTP is observed. However, the location of an additional methyl group on the nucleotide base can affect activity. Both *Mt*MutT2 and Orf135 can hydrolyze 5-methyl-dCTP, but neither is capable of hydrolyzing 4-methyl-dCTP (Figure 4A (*27*)). Limited hydrolysis of dTTP by *Mt*MutT2 is observed, which also has a methyl group at the C5 position, suggesting that there is room in the active site to accommodate a 5-methyl but not a 4-methyl group on the nucleotide base.

The proposed nucleotide binding site of *Mt*MutT2 is relatively distant from Gly-58 in the homology model (Figure 2B), explaining why nucleotide specificity is unaltered in G58R. The structure of *Ec*MutT bound with 8-oxo-dGMP, the hydrolysis product of its preferred substrate 8-oxo-dGTP (Figure 2A), shows that the nucleotide binding site comprises a large hydrophobic cleft on the β-sheet some distance away from Gly-59 (the corresponding residue to Gly-58 in *Mt*-MutT2). Several residues have been shown to interact with substrate in *Ec*MutT, including Asn-119, which hydrogen bonds with the purine ring, and Lys-39 which interacts with the α-phosphate of 8-oxo-dGMP (Figure 2C (*23*)). Lys-39 is conserved in *Mt*MutT2 and Orf135 (Figures 1 and 2B) and mutations of this residue to alanine in Orf135 drastically reduced cytidine triphosphatase activity, confirming a role in substrate binding (*29, 36*). The residue equivalent to Asn-119 in *Mt*MutT2 and Orf135 is an aspartate (Asp-119 and Asp-118, respectively; Figures 1 and 2B). Since the asparagine in *Ec*MutT interacts directly with the purine ring of the substrate, this residue may be involved in determining nucleotide specificity. Mutating this residue to an aspartate (N119D) significantly weakened the binding of 8-oxo-dGMP to *Ec*MutT (*37*). The reverse mutation in Orf135 (D118N) reduced hydrolysis of dCTP and overall catalytic efficiency (k_{cat}/K_m) by approximately half (*36*). Similarly, when we mutated Asp-119 to an asparagine (D119N) in *Mt*MutT2 we observed a decrease in dCTP hydrolysis of over 50% compared with that of the wild-type (data not shown). Taken together, these results suggest that the carboxyl group (COO^-) of an aspartate at this position is necessary for binding to cytidine, whereas the amide moiety ($CONH_2$) of an asparagine selects for guanosine binding. Asn-119 in *Ec*MutT has been shown to donate one hydrogen bond to 8-oxo-GMP and accept another (*37*), while the aspartate in *Mt*MutT2 and Orf135 would accept two hydrogen bonds from dCTP. This is illustrated in Figure 2C.

Divalent Metal Requirement Is Increased in the G58R Mutant. The metal dependence of wild-type and G58R *Mt*MutT2 was monitored using the modified colorimetric method (*18*) and dCTP as substrate. As with *Ec*MutT (*21*), little or no activity is detected for *Mt*MutT2 until the concentration of magnesium exceeds that of the nucleotide (2.5 mM, Figure 4B). *Ec*MutT-catalyzed hydrolysis requires two divalent cations, one coordinated by the conserved Nudix residues and a second that is coordinated to the nucleotide triphosphate (NTP) substrate via the β- and γ-phosphates (Figure 2C). The relatively low dissociation constant for metal nucleotide complexes (approximately 10 μM) means magnesium is not available to bind the Nudix residues until the metal concentration exceeds the NTP concentration. When the titration curves for *Mt*MutT2 are corrected for nucleotide bound Mg^{2+} and plotted against the concentration of free magnesium (Figure 4B), the reaction becomes hyperbolic. This is also observed with *Ec*MutT when activity is plotted as a function of total and free magnesium, respectively, and is evidence of a metal-bound nucleotide (*21*).

The substrate screen was performed at a saturating concentration of Mg^{2+} (15 mM), and under these conditions, there was no significant difference in hydrolysis between the wild-type and G58R *Mt*MutT2 (Figure 4A). However, the Mg^{2+} titration shows a clear difference in Mg^{2+} requirement between the wild-type and G58R (Figure 4B). The wild-type enzyme displays maximal hydrolysis at 5 mM Mg^{2+}, whereas the mutant does not reach maximal hydrolysis until 15 mM Mg^{2+}. Kinetic analysis, to determine affinity for free Mg^{2+}, also showed significant differences between the wild-type and G58R *Mt*MutT2 enzymes. Protein concentrations were kept constant, substrate concentration (dCTP) was

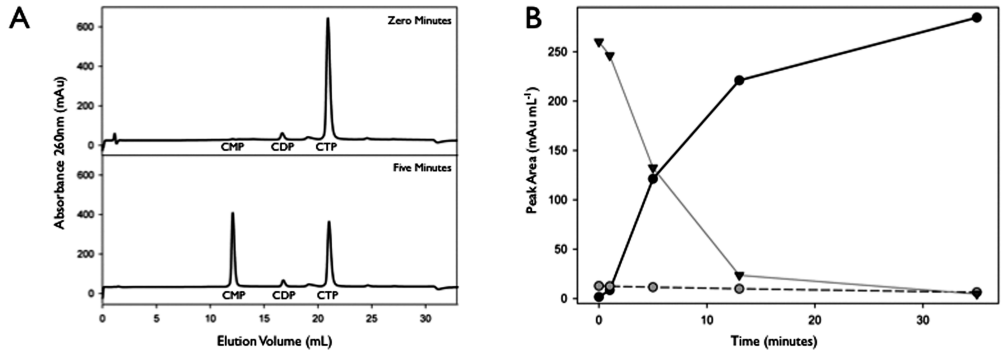

FIGURE 5: Products of the reaction of wild-type *Mt*MutT2 with CTP. (A) Product formation monitored by anion-exchange HPLC with detection at 260 nm. (B) The area under each elution peak (mAu mL^{-1}) was calculated to quantify the levels of CTP (▼), CDP (gray circle), and CMP (●).

saturating, and Mg^{2+} concentration was varied (0−50 mM). The Mg^{2+} concentration was corrected for nucleotide bound Mg^{2+} using a K_D of 10 μM for Mg^{2+}-dCTP. The K_D of free Mg^{2+} is 79-fold higher for the G58R mutant (3.30 ± 0.19 mM) compared with that of the wild-type (41.7 ± 1.4 μM), showing that the metal binding capability of G58R has been greatly affected by the introduction of the bulky arginine residue in the Nudix box. The homology model for *Mt*MutT2 (Figure 2B) suggests that this is due to the proximity of Gly-58 to the residues involved in Mg^{2+} coordination in the Nudix box (Gly-37 and Glu-52, Glu-55 and Glu-56); the distance from the α-carbon of Gly-58 to the Mg^{2+} is 10.8 Å.

Product Formation Following CTP Hydrolysis. The hydrolysis products formed by incubation of CTP with *Mt*MutT2 were monitored by anion-exchange HPLC as previously described (*22*). As seen in Figure 5A, the method clearly separates CTP from its corresponding mono- and diphosphate forms. Following a five-minute incubation of wild-type *Mt*MutT2 with CTP, a marked increase in the area of the CMP peak is observed. There is no change in the CDP peak compared with time zero (Figure 5A). Over a 35-min time period, the concentration of CMP continued to increase, and no CDP formation was detected (Figure 5B). An incubation of the G58R mutant with CTP also resulted in an increase in CMP and no change in CDP concentration (data not shown).

The products formed are the same as those observed when Orf135 is incubated with CTP (*27*). *Ec*MutT has been shown to hydrolyze dGTP to dGMP (*35*), and in general, Nudix enzymes hydrolyze the α-β phosphate bond to yield a monophosphorylated product (*11, 12*). Protein NMR studies utilizing the paramagnetic effects of Co^{2+}, ^{31}P NMR spectroscopy in $H_2{}^{18}O$ water, and site-directed mutagenesis have been used to determine the contribution of certain *Ec*MutT residues to enzyme-catalyzed hydrolysis of the α-β phosphate bond (*12, 38*). Of the residues involved in substrate binding (Lys-39 and Asn-119) and divalent cation binding (Gly-38, Glu-53, Glu-56, and Glu-57), it is the glutamates in the Nudix box, and in particular Glu-53 and Glu-57, which have been shown to be most critical for catalysis. It is thought that a water ligand, involved in coordinating the divalent cation with the conserved Nudix box residues (Figure 2A), attacks the β phosphate of the NTP resulting in hydrolysis. Glu-53 and Glu-57 are thought to be crucial for correct positioning of the divalent cation and, in turn, the water ligand, to ensure displacement of the β phosphate occurs. Given the conservation of Nudix box residues between *Ec*MutT and *Mt*MutT2, and the formation of a monophosphorylated product following incubation of *Mt*MutT2 with CTP, it is likely that the corresponding residues in *Mt*MutT2 (Glu-52 and Glu-56; Figure 2B) are similarly crucial for hydrolysis of the α-β phosphate bond.

Table 1: Kinetic Parameters for Wild-Type and G58R Mutant *Mt*MutT2 with dCTP[a]

	K_m (mM)	k_{cat} (s^{-1})	k_{cat}/K_m (M^{-1} s^{-1}) × 10^2
wild-type	2.60 ± 0.51	1.72 ± 0.14	6.63 ± 1.17
G58R	0.72 ± 0.27	0.55 ± 0.06	7.55 ± 0.70

[a] k_{cat} was calculated from V_{max}. All values are means ± S.E.M.

Kinetic Properties of the Wild-Type and G58R MtMutT2. A kinetic analysis of wild-type and G58R *Mt*MutT2 with one of the preferred substrates (dCTP) was performed using the modified colorimetric method (*18*). The Mg^{2+} concentration was saturating (15 mM), protein concentrations were kept constant, and substrate concentration was varied (0−7.5 mM). Although the wild-type enzyme hydrolyses dCTP approximately three times faster (k_{cat} 1.72 s^{-1}) than the G58R mutant (k_{cat} 0.55 s^{-1}), there is no significant difference in the overall catalytic efficiency of the two due to the smaller apparent K_m value for G58R (0.72 mM) compared with wild-type (2.60 mM) (Table 1). These K_m values are comparable to those reported for Orf135 with dCTP in two separate studies; 0.77 mM and 0.99 mM (*27, 29*).

The lower rate of dCTP hydrolysis in the G58R mutant compared with wild-type is most likely a result of pertubations in the metal binding site of G58R. As discussed above, Glu-52 and Glu-56, which coordinate Mg^{2+} in the *Mt*MutT2 homology model (Figure 2B), are thought to play a key role in catalysis by correctly positioning a water ligand for phosphate bond hydrolysis. The proximity of Gly-58 to these metal binding residues and the higher concentration of Mg^{2+} required by the G58R mutant for NTP hydrolysis (Figure 4B) suggest that the arginine substitution has affected the metal binding site in G58R. Any change in the conformation of Glu-52 and Glu-56 would impact on positioning of the water ligand and enzyme-catalyzed hydrolysis of the phosphate bond. The lower K_m for G58R is harder to explain, and while it may suggest tighter substrate binding, this is complicated by the reaction mechanism. *Ec*MutT catalyzed hydrolysis has been shown to occur via an iso-uni-bi kinetic mechanism such that the K_m of the substrate is not a dissociation constant, but contains at least seven rate constants (*12*). It is likely that *Mt*MutT2 catalyzed hydrolysis

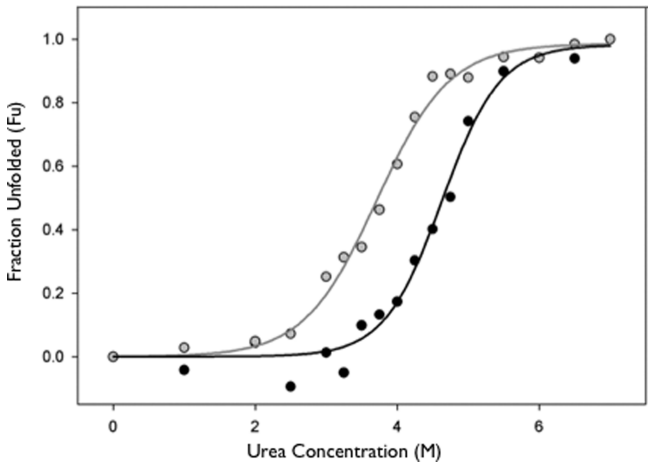

FIGURE 6: Urea denaturation of wild-type (black) and G58R (gray) *Mt*MutT2 monitored by far-UV circular dichroism (218 nm).

Table 2: Parameters Characterising the Urea Unfolding Curves of Wild-Type and G58R *Mt*MutT2 Derived Using the Two-State Model and the Linear Extrapolation Method[a]

	C_m (M)	ΔG (H_2O) (kcal mol^{-1})	*m*-value (kcal mol^{-1} M^{-1})
wild-type	4.57	7.04	1.54
G58R	3.68	4.56	1.24

[a] All values were calculated using fitted data. R^2 values for curve fitting are 0.988 (wild-type) and 0.992 (G58R).

occurs via a similar mechanism making the K_m of dCTP difficult to interpret in isolation. Over and above this, the 79-fold increase in K_D of free Mg^{2+} observed for the G58R mutant should be considered. This is likely to have a much greater impact on activity *in vivo* than the modest decrease in K_m for dCTP.

Wild-Type MtMutT2 Is More Stable Than G58R. The stabilities of wild-type and G58R mutant *Mt*MutT2 were measured by monitoring the CD signal at 218 nm during unfolding with urea. Unfolding experiments were performed at least three times for both the wild-type and G58R proteins, and typical results are shown in Figure 6. The transition curves were fitted using SigmaPlot (R^2 for wild-type and G58R are 0.988 and 0.992, respectively) with the sigmoidal change in the curves being indicative of two-state unfolding. The unfolding of wild-type and G58R was shown to be reversible, and transition curves were analyzed using the linear extrapolation method (*15*). The concentration of urea at which half the protein is unfolded (C_m) is markedly lower for G58R (3.68 M) compared with that of the wild-type (4.57 M). Similarly, the stability (ΔG (H_2O)) of G58R (4.56 kcal mol^{-1}) is reduced by 2.48 kcal mol^{-1} compared with that of the wild-type (7.04 kcal mol^{-1}) demonstrating that the introduction of an arginine destabilizes *Mt*MutT2 (Table 2). Interestingly, the *m*-value for G58R is 20% lower than that for wild-type (1.24 compared with 1.54 kcal mol^{-1} M^{-1}). As the *m*-value is proportional to the number of groups in a protein exposed to solvent in the denatured state (*15*), it follows that additional residues in G58R remain inaccessible to solvent when the protein is unfolded. This suggests that the introduction of an aginine affects not only protein stability but also the nature of the unfolded state of *Mt*MutT2.

The large decrease in stability seen in the G58R mutant suggests that Gly-58 is necessary to maintain a stable structure. Gly-58 forms part of a tight turn following the conserved helix in our homology model and, as discussed earlier, falls in a region of the Ramachandran plot that is disallowed for nonglycine residues. Analysis of modeled *Mt*MutT2 indicates that a geometrically favorable backbone hydrogen bond is formed between Gly-58 and Ala-54 (Figure 2B). A hydrogen bond is also seen at this position in *Ec*MutT (between Gly-59 and Gln-55). When arginine was substituted for Gly-58 in the *Mt*MutT2 model and the model energy minimized, a change in backbone conformation from (φ = 61 °, Ψ = −55 °) to (φ = 72 °, Ψ = −8 °) was observed to accommodate the bulky arginine side chain. Arg-58 was then located in the additionally allowed region of the Ramachandran plot, and while its peptide nitrogen was still able to form a hydrogen bond with the carbonyl oxygen of Ala-54, the geometry was markedly less favorable (N−H...O angle of 115° for Arg-58 compared with 150° for Gly-58). Weakening of this backbone hydrogen bond may explain the reduced stability observed for the G58R mutant *in vitro*.

Mutational studies with the human homologue of *Ec*MutT (MTH1) have also demonstrated a destabilizing effect following substitution of a glycine by arginine at this position (*39*). Although sequence identity between *Mt*MutT2 and MTH1 is relatively low (18%), the conserved Nudix box shows a high level of identity (56%), and Gly-58 in MTH1 also forms part of a tight turn following the conserved helix (*40*). The G58R mutant of MTH1 possessed substantial 8-oxo-dGTPase activity, but the expression of the protein in cells was significantly reduced compared with that of the wild-type. The authors suggest that this is due to protein destabilization, with Gly-58 being integral in maintaining a stable MTH1 structure *in vivo* (*39*).

CONCLUDING REMARKS

*Mt*MutT2 has a preference for cytidine triphosphates rather than guanosine triphosphates and is thus unlikely to function as a DNA repair enzyme by hydrolyzing the damaged nucleotide 8-oxo-dGTP, nor contribute to a mutator phenotype in W-Beijing strains as previously proposed (*3, 4*). The specificity for cytidine triphosphates is the same as that observed for Orf135 (*27*), and although Orf135 has been well characterized *in vitro*, there have been no *in vivo* studies investigating cellular function to date. What then are the possible roles of *Mt*MutT2 and other cytidine specific Nudix hydrolases in the cell? The preferred substrates for *Mt*MutT2 *in vitro* are dCTP, CTP, and 5-methyl-dCTP, and *Mt*MutT2 may regulate the levels of these or other cytidine triphosphate analogues *in vivo.* Nucleotides are essential for RNA synthesis and DNA replication, and CTP is a key metabolite in both pyrimidine and polysaccharide synthesis (*41*). By controlling the levels of cytidine triphosphates available for central cellular pathways (via hydrolysis to a monophosphorylated product), *Mt*MutT2 may function as part of a network of enzymes that regulate nucleotide-dependent processes. In *E. coli*, Nudix hydrolases have been identified with specificity for each of the four major NTPs (*11, 42*). It is possible that among the nine sequences containing Nudix box amino acids we identified in an initial BLAST search of the *M. tuberculosis* genome there are Nudix hydrolases with nucleotide specificities to complement *Mt*MutT2.

*Mt*MutT2 is upregulated 2-fold in a nutrient starvation model of *M. tuberculosis* that is thought to mimic the

persistent state of the bacterium observed *in vivo* (*43*). Viable bacilli residing within granulomas in the lungs of tuberculosis patients are maintained in a dormant state through conditions such as low oxygen tension and nutrient limitation. The nutrient starvation model showed a slowing of transcriptional apparatus, energy metabolism, lipid biosynthesis, and cell division. A 2-fold upregulation of *Mt*MutT2 and the concomitant drop in cytidine-triphosphates available for nucleotide-dependent cellular processes this may induce are consistent with the general slowdown of metabolism observed in the persistent state.

What impact would the observed differences between the wild-type and G58R proteins have on *Mt*MutT2 function in W-Beijing strains *in vivo*? The large protein destabilization effect caused by the arginine substitution would result in decreased levels of *Mt*MutT2 in the cell, and the protein that remains is likely to hydrolyze cytidine triphosphates in a less efficient manner because of a significantly reduced affinity for Mg^{2+} and a 3-fold reduction in k_{cat}. The physiological concentration of free Mg^{2+} in bacteria has been estimated as approximately 1 mM (*44, 45*). The K_D of the G58R mutant for free Mg^{2+} is higher than this (3.30 ± 0.19 mM), whereas that of the wild-type is significantly lower (41.7 ± 1.4 μM). This suggests that the wild-type enzyme would normally be saturated with Mg^{2+}, but not all of the mutant enzyme would be bound to catalytically essential Mg^{2+} in W-Beijing strains. If the role of *Mt*MutT2 were to regulate the levels of cytidine-triphosphate available for cellular processes (by hydrolysis to the monophosphate), then W-Beijing strains expressing the G58R mutant protein would have higher levels of cytidine-triphosphates in their nucleotide pool. This may enable the bacterium to perform nucleotide-dependent reactions when environmental cues such as nutrient starvation would normally stop these from occurring. Interestingly, some W-Beijing strains have shown increased replication rates within *in vitro* grown macrophages (*46*−*48*) suggesting an increase in nucleotide-dependent reactions may be one of the many features that contribute to the global success of these strains.

ACKNOWLEDGMENT

We thank Drs. Harriet Watkins and Esther Bulloch for assay advice and Dr. Mojtaba Amani for help with circular dichroism.

REFERENCES

1. Abebe, F., and Bjune, G. (2006) The emergence of Beijing family genotypes of *Mycobacterium tuberculosis* and low-level protection by bacille Calmette-Guérin (BCG) vaccines: is there a link? *Clin. Exp. Immunol. 145*, 389–397.
2. Glynn, J. R., Whiteley, J., Bifani, P. J., Kremer, K., and van Soolingen, D. (2002) Worldwide occurrence of Beijing/W strains of *Mycobacterium tuberculosis*: a systematic review. *Emerging Infect. Dis. 8*, 843–849.
3. Lari, N., Rindi, L., Bonanni, D., Tortoli, E., and Garzelli, C. (2006) Mutations in mutT genes of *Mycobacterium tuberculosis* isolates of Beijing genotype. *J. Med. Microbiol. 55*, 599–603.
4. Rad, M. E., Bifani, P., Martin, C., Kremer, K., Samper, S., Rauzier, J., Kreiswirth, B., Blazquez, J., Jouan, M., van Soolingen, D., and Gicquel, B. (2003) Mutations in putative mutator genes of *Mycobacterium tuberculosis* strains of the W-Beijing family. *Emerging Infect. Dis. 9*, 838–845.
5. Ramaswamy, S., and Musser, J. M. (1998) Molecular genetic basis of antimicrobial agent resistance in *Mycobacterium tuberculosis*: 1998 update. *Tuber Lung Dis. 79*, 3–29.
6. Ramaswamy, S. V., Reich, R., Dou, S. J., Jasperse, L., Pan, X., Wanger, A., Quitugua, T., and Graviss, E. A. (2003) Single nucleotide polymorphisms in genes associated with isoniazid resistance in *Mycobacterium tuberculosis*. *Antimicrob. Agents Chemother. 47*, 1241–1250.
7. Cole, S. T., Brosch, R., Parkhill, J., Garnier, T., Churcher, C., Harris, D., Gordon, S. V., Eiglmeier, K., Gas, S., Barry, C. E., Tekaia, F., Badcock, K., Basham, D., Brown, D., Chillingworth, T., Connor, R., Davies, R., Devlin, K., Feltwell, T., Gentles, S., Hamlin, N., Holroyd, S., Hornsby, T., Jagels, K., Krogh, A., McLean, J., Moule, S., Murphy, L., Oliver, K., Osborne, J., Quail, M. A., Rajandream, M. A., Rogers, J., Rutter, S., Seeger, K., Skelton, J., Squares, R., Squares, S., Sulston, J. E., Taylor, K., Whitehead, S., and Barrell, B. G. (1998) Deciphering the biology of *Mycobacterium tuberculosis* from the complete genome sequence. *Nature 393*, 537–544.
8. Mizrahi, V., and Andersen, S. J. (1998) DNA repair in *Mycobacterium tuberculosis*. What have we learnt from the genome sequence? *Mol. Microbiol. 29*, 1331–1339.
9. Maki, H., and Sekiguchi, M. (1992) MutT protein specifically hydrolyses a potent mutagenic substrate for DNA synthesis. *Nature 355*, 273–275.
10. Galperin, M., Moroz, O., Wilson, K., and Murzin, A. (2006) House cleaning, a part of good housekeeping. *Mol. Microbiol. 59*, 5–19.
11. McLennan, A. G. (2006) The Nudix hydrolase superfamily. *Cell. Mol. Life Sci. 63*, 123–143.
12. Mildvan, A. S., Xia, Z., Azurmendi, H. F., Saraswat, V., Legler, P. M., Massiah, M. A., Gabelli, S. B., Bianchet, M. A., Kang, L. W., and Amzel, L. M. (2005) Structures and mechanisms of Nudix hydrolases. *Arch. Biochem. Biophys. 433*, 129–143.
13. Moreland, N., Ashton, R., Baker, H. M., Ivanovic, I., Patterson, S., Arcus, V. L., Baker, E. N., and Lott, J. S. (2005) A flexible and economical medium-throughput strategy for protein production and crystallization. *Acta Crystallogr., Sect. D 61*, 1378–1385.
14. Studier, F. W. (2005) Protein production by auto-induction in high density shaking cultures. *Protein Expression Purif. 41*, 207–234.
15. Pace, C. N., and Shaw, K. L. (2000) Linear extrapolation method of analyzing solvent denaturation curves. *Proteins Suppl. 4*, 1–7.
16. Delaglio, F., Grzesiek, S., Vuister, G. W., Zhu, G., Pfeifer, J., and Bax, A. (1995) NMRPipe: a multidimensional spectral processing system based on UNIX pipes. *J. Biomol. NMR 6*, 277–293.
17. Vranken, W. F., Boucher, W., Stevens, T. J., Fogh, R. H., Pajon, A., Llinas, M., Ulrich, E. L., Markley, J. L., Ionides, J., and Laue, E. D. (2005) The CCPN data model for NMR spectroscopy: development of a software pipeline. *Proteins 59*, 687–696.
18. Ames, B. N., and Dubin, D. T. (1960) The role of polyamines in the neutralization of bacteriophage deoxyribonucleic acid. *J. Biol. Chem. 235*, 769–775.
19. Du Peloux, C., Mialane, P., Dolbecq, A., Marrot, J., and Sécheresse, F. (2002) Mo(V)/pyrophosphate polyoxometalate: an inorganic cryptate. *Angew. Chem., Int. Ed. 41*, 2808–2810.
20. Flynn, R. M., Jones, M. E., and Lipmann, F. (1954) A colorimetric determination of inorganic pyrophosphate. *J. Biol. Chem. 211*, 791–796.
21. Frick, D. N., Weber, D. J., Gillespie, J. R., Bessman, M. J., and Mildvan, A. S. (1994) Dual divalent cation requirement of the MutT dGTPase. Kinetic and magnetic resonance studies of the metal and substrate complexes. *J. Biol. Chem. 269*, 1794–1803.
22. Tomiya, N., Ailor, E., Lawrence, S. M., Betenbaugh, M. J., and Lee, Y. C. (2001) Determination of nucleotides and sugar nucleotides involved in protein glycosylation by high-performance anion-exchange chromatography: sugar nucleotide contents in cultured insect cells and mammalian cells. *Anal. Biochem. 293*, 129–137.
23. Massiah, M. A., Saraswat, V., Azurmendi, H. F., and Mildvan, A. S. (2003) Solution structure and NH exchange studies of the MutT pyrophosphohydrolase complexed with Mg(2+) and 8-oxo-dGMP, a tightly bound product. *Biochemistry 42*, 10140–10154.
24. Lambert, C., Léonard, N., De Bolle, X., and Depiereux, E. (2002) ESyPred3D: Prediction of proteins 3D structures. *Bioinformatics 18*, 1250–1256.
25. Sali, A., Potterton, L., Yuan, F., van Vlijmen, H., and Karplus, M. (1995) Evaluation of comparative protein modeling by MODELLER. *Proteins 23*, 318–326.
26. Goodford, P. J. (1985) A computational procedure for determining energetically favorable binding sites on biologically important macromolecules. *J. Med. Chem. 28*, 849–857.
27. O'Handley, S. F., Dunn, C. A., and Bessman, M. J. (2001) Orf135 from *Escherichia coli* is a Nudix hydrolase specific for CTP, dCTP, and 5-methyl-dCTP. *J. Biol. Chem. 276*, 5421–5426.

28. Abeygunawardana, C., Weber, D. J., Gittis, A. G., Frick, D. N., Lin, J., Miller, A. F., Bessman, M. J., and Mildvan, A. S. (1995) Solution structure of the MutT enzyme, a nucleoside triphosphate pyrophosphohydrolase. *Biochemistry 34*, 14997–15005.
29. Kamiya, H., Iida, E., and Harashima, H. (2004) Important amino acids in the phosphohydrolase module of *Escherichia coli* Orf135. *Biochem. Biophys. Res. Commun. 323*, 1063–1068.
30. Abeygunawardana, C., Weber, D. J., Frick, D. N., Bessman, M. J., and Mildvan, A. S. (1993) Sequence-specific assignments of the backbone 1H, 13C, and 15N resonances of the MutT enzyme by heteronuclear multidimensional NMR. *Biochemistry 32*, 13071–13080.
31. Greenfield, N. J. (2006) Using circular dichroism spectra to estimate protein secondary structure. *Nature protocols 1*, 2876–2890.
32. Böhm, G., Muhr, R., and Jaenicke, R. (1992) Quantitative analysis of protein far UV circular dichroism spectra by neural networks. *Protein Eng. 5*, 191–195.
33. Galvão-Botton, L. M., Katsuyama, A. M., Guzzo, C. R., Almeida, F. C., Farah, C. S., and Valente, A. P. (2003) High-throughput screening of structural proteomics targets using NMR. *FEBS Lett. 552*, 207–213.
34. Wishart, D. S., and Sykes, B. D. (1994) Chemical shifts as a tool for structure determination. *Methods Enzymol. 239*, 363–392.
35. Bhatnagar, S. K., Bullions, L. C., and Bessman, M. J. (1991) Characterization of the MutT nucleoside triphosphatase of *Escherichia coli*. *J. Biol. Chem. 266*, 9050–9054.
36. Iida, E., Satou, K., Mishima, M., Kojima, C., Harashima, H., and Kamiya, H. (2005) Amino acid residues involved in substrate recognition of the *Escherichia coli* Orf135 protein. *Biochemistry 44*, 5683–5689.
37. Saraswat, V., Azurmendi, H. F., and Mildvan, A. S. (2004) Mutational, NMR, and NH exchange studies of the tight and selective binding of 8-oxo-dGMP by the MutT pyrophosphohydrolase. *Biochemistry 43*, 3404–3414.
38. Weber, D. J., Bhatnagar, S. K., Bullions, L. C., Bessman, M. J., and Mildvan, A. S. (1992) NMR and isotopic exchange studies of the site of bond cleavage in the MutT reaction. *J. Biol. Chem. 267*, 16939–16942.
39. Fujii, Y., Shimokawa, H., Sekiguchi, M., and Nakabeppu, Y. (1999) Functional significance of the conserved residues for the 23-residue module among MTH1 and MutT family proteins. *J. Biol. Chem. 274*, 38251–38259.
40. Mishima, M., Sakai, Y., Itoh, N., Kamiya, H., Furuichi, M., Takahashi, M., Yamagata, Y., Iwai, S., Nakabeppu, Y., and Shirakawa, M. (2004) Structure of human MTH1, a Nudix family hydrolase that selectively degrades oxidized purine nucleoside triphosphates. *J. Biol. Chem. 279*, 33806–33815.
41. Chakrabarty, A. M. (1998) Nucleoside diphosphate kinase: role in bacterial growth, virulence, cell signalling and polysaccharide synthesis. *Mol. Microbiol. 28*, 875–882.
42. Xu, W., Shen, J., Dunn, C. A., and Bessman, M. J. (2003) A new subfamily of the Nudix hydrolase superfamily active on 5-methyl-UTP (ribo-TTP) and UTP. *J. Biol. Chem. 278*, 37492–37496.
43. Betts, J. C., Lukey, P. T., Robb, L. C., McAdam, R. A., and Duncan, K. (2002) Evaluation of a nutrient starvation model of *Mycobacterium tuberculosis* persistence by gene and protein expression profiling. *Mol. Microbiol. 43*, 717–731.
44. Chang, C. F., Shuman, H., and Somlyo, A. P. (1986) Electron probe analysis, X-ray mapping, and electron energy-loss spectroscopy of calcium, magnesium, and monovalent ions in log-phase and in dividing *Escherichia coli* B cells. *J. Bacteriol. 167*, 935–939.
45. Klaus, S. M., Wegkamp, A., Sybesma, W., Hugenholtz, J., Gregory, J. F., and Hanson, A. D. (2005) A nudix enzyme removes pyrophosphate from dihydroneopterin triphosphate in the folate synthesis pathway of bacteria and plants. *J. Biol. Chem. 280*, 5274–5280.
46. Barczak, A. K., Domenech, P., Boshoff, H. I., Reed, M. B., Manca, C., Kaplan, G., and Barry, C. E. (2005) In vivo phenotypic dominance in mouse mixed infections with *Mycobacterium tuberculosis* clinical isolates. *J. Infect. Dis. 192*, 600–606.
47. Li, Q., Whalen, C. C., Albert, J. M., Larkin, R., Zukowski, L., Cave, M. D., and Silver, R. F. (2002) Differences in rate and variability of intracellular growth of a panel of *Mycobacterium tuberculosis* clinical isolates within a human monocyte model. *Infect. Immun. 70*, 6489–6493.
48. Reed, M. B., Gagneux, S., Deriemer, K., Small, P. M., and Barry, C. E. (2007) The W-Beijing lineage of *Mycobacterium tuberculosis* overproduces triglycerides and has the DosR dormancy regulon constitutively upregulated. *J. Bacteriol. 189*, 2583–2589.
49. Thompson, J. D., Higgins, D. G., and Gibson, T. J. (1994) CLUSTAL W: improving the sensitivity of progressive multiple sequence alignment through sequence weighting, position-specific gap penalties and weight matrix choice. *Nucleic Acids Res. 22*, 4673–4680.
50. McGuffin, L. J., Bryson, K., and Jones, D. T. (2000) The PSIPRED protein structure prediction server. *Bioinformatics 16*, 404–405.

BI8009554